Available online at www.sciencedirect.com

ScienceDirect

Advances in Space Research 56 (2015) 190–204

ADVANCES IN SPACE RESEARCH (a COSPAR publication)

www.elsevier.com/locate/asr

# Twilight on Ligeia: Implications of communications geometry and seasonal winds for exploring Titan's seas 2020–2040

Ralph D. Lorenz [a,*], Claire E. Newman [b]

[a] Johns Hopkins University Applied Physics Laboratory, 11100 Johns Hopkins Road, Laurel, MD 20723, USA
[b] Ashima Research, 600 S. Lake Ave., Suite 303, Pasadena, CA 91106, USA

Received 3 December 2014; received in revised form 9 March 2015; accepted 23 March 2015
Available online 1 April 2015

**Abstract**

Titan's lakes and seas are targets of particular interest for future exploration. We review candidate splashdown areas in Ligeia and Kraken Mare, and Ontario Lacus. Titan's thick and dense atmosphere means that landing dispersions of spacecraft are dominated by uncertainties in wind drift, and thus the feasibility of landing safely in the sea with a simple Huygens-like descent system (i.e. without guidance or propulsion) is dependent upon these uncertainties being small enough that the landing point dispersion lies within the sea. Because Titan's winds vary with season, notably through the formation of a high-speed stratospheric jet in the winter hemisphere, landing point dispersions are seasonally-dependent as well as latitude-dependent. Ligeia Mare, at 78°N, sees relatively small dispersions but offers viable Direct-to-Earth (DTE) communication only until 2024. A wide part of Kraken Mare (450 × 90 km) at 70°N can be comfortably reached at all times, and is viable for assured Direct-to-Earth communication until 2026, or with a relay spacecraft thereafter. The seasonal geometry permits DTE from the northern seas again after 2040. Wind dispersions are always too large for Ontario, unless a steerable parachute or similar system is used to tighten the landing ellipse.


*Keywords:* Titan; Mission design; Direct-to-Earth communications; Wind dispersions; Navigation

## 1. Introduction

Among Titan's many interesting features such as dunes and river channels revealed by the Cassini–Huygens mission (e.g. Lorenz and Mitton, 2010; Coustenis and Taylor, 2008; Brown et al., 2009), perhaps the most striking aspect is Titan's geographical diversity and in particular that there are major and systematic variations with latitude of the character of the surface and the properties of the atmosphere. Of these variations, most remarkable is the presence of large and persistent bodies of hydrocarbon liquids at high latitudes and especially the north. These seas and lakes have attracted great interest as targets for future exploration, most recently as the Titan Mare Explorer (TiME) Discovery mission concept (Stofan et al., 2013, Fig. 1) but also the National Research Council/NASA Decadal Survey Titan Lake Lander circa 2010 (JPL, 2010 – see also Space Studies Board, 2012), and a landed element in the NASA–ESA TSSM (Titan Saturn System Mission) study of 2008 (ESA, 2009; Reh and Elliott, 2010), as well as more recent ideas (Mitri et al., 2014). In addition to the scientific appeal of in situ study of Earth-like air–sea interactions and a major volatile reservoir and chemical deposit of astrobiological interest, Titan's seas offer the practical convenience of safe landing by splashdown and thereby avoid the need to provide retropropulsion, impact attenuation by airbag or other systems that would be costly to develop and test for the Titan environment. However, to exploit splashdown obviously

* Corresponding author. Tel.: +1 443 778 2903; fax: +1 443 778 8939.
*E-mail address:* ralph.lorenz@jhuapl.edu (R.D. Lorenz).

http://dx.doi.org/10.1016/j.asr.2015.03.034
0273-1177/

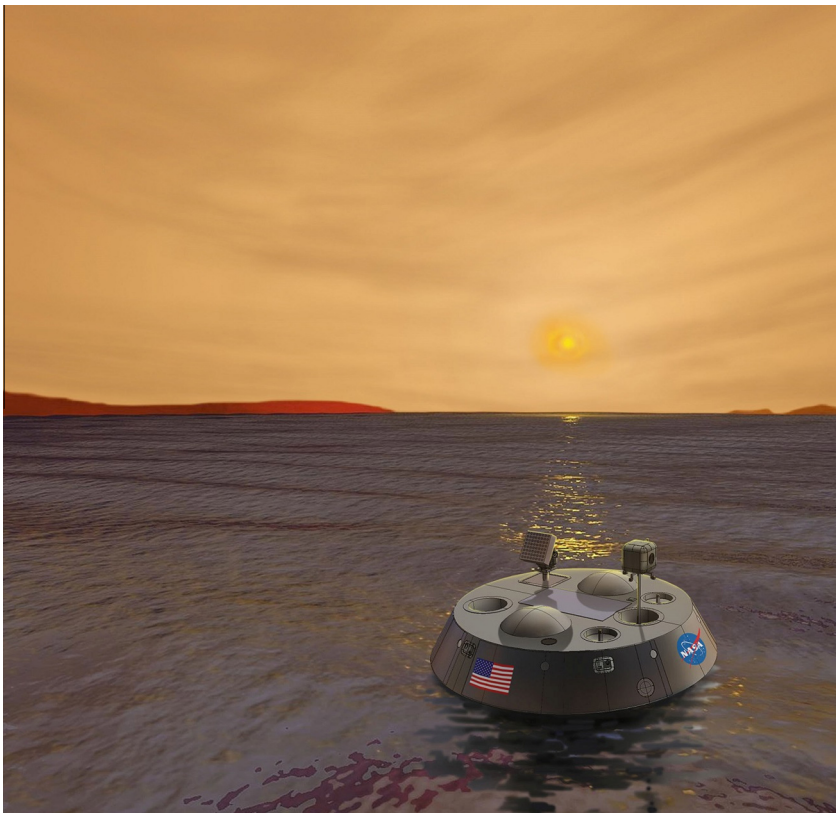

Fig. 1. Artist's concept of the Titan Mare Explorer (TiME) mission, as conceived at the beginning of the Phase A study (May 2011). An instrumented capsule, with a camera and planar communications antenna, is shown on Ligeia Mare, with the sun low in the sky. Image: Johns Hopkins Applied Physics Laboratory/Lockheed Martin.

requires that the vehicle land at sea, and doing so requires quantitative consideration of the target areas involved and the dispersion of the splashdown points by the wind profile.

Because of Titan's effective obliquity (actually, largely due to Saturn's obliquity of 26.7°), the polar regions see considerable seasonal variation of solar and earth elevation. This directly influences illumination, and the possibility of Direct-to-Earth communication, and indirectly influences winds, which (especially in the stratosphere) change significantly with season.

A previous paper (Lorenz et al., 2012a), informed by Cassini and groundbased observations and four independent Global Circulation Models (GCMs), summarized northern summer polar wind conditions (specifically, regions north of 70°N, during the 2023–2024 period, or solar longitude $L_s \sim 150°$–$170°$) and presented a simple analytical formulation of expected, minimum and maximum winds as a function of altitude, with specific reference to the Titan Mare Explorer (TiME) Discovery mission (Fig. 1). The present paper considers (and quantifies) a broader range of target locations and seasons to inform prospects for future missions to Titan's seas, in which considerable interest remains (e.g. Mitri et al. (2014)).

## 2. Geographic and astronomical context

Titan's seas, while anticipated before Cassini, were only revealed (in winter darkness) over two years after Cassini's arrival. Mapping (Fig. 2) by radar showed (Stofan et al., 2007; Lopes et al., 2007; Aharonson et al., 2009; Lorenz et al. 2014) many small lakes around Titan's north pole, and then three major seas (in order of increasing size, Punga Mare, Ligeia Mare and Kraken Mare). These are also now being mapped in the near-infrared (e.g. Sotin et al. (2012)) as we move towards northern summer. The southern hemisphere lacks such seas, having only one major lake (Ontario Lacus).

### 2.1. Target areas and tolerable footprints

We consider four target areas. The first is Ligeia Mare, the nominal target of the TiME mission. Being the northernmost, however, this becomes unusable for Direct-to-Earth communication earliest as the sub-Earth point migrates south in the 2020s. The next two are regions of Kraken Mare: this body – the largest sea on Titan – is somewhat irregular in shape (which may lead to interesting

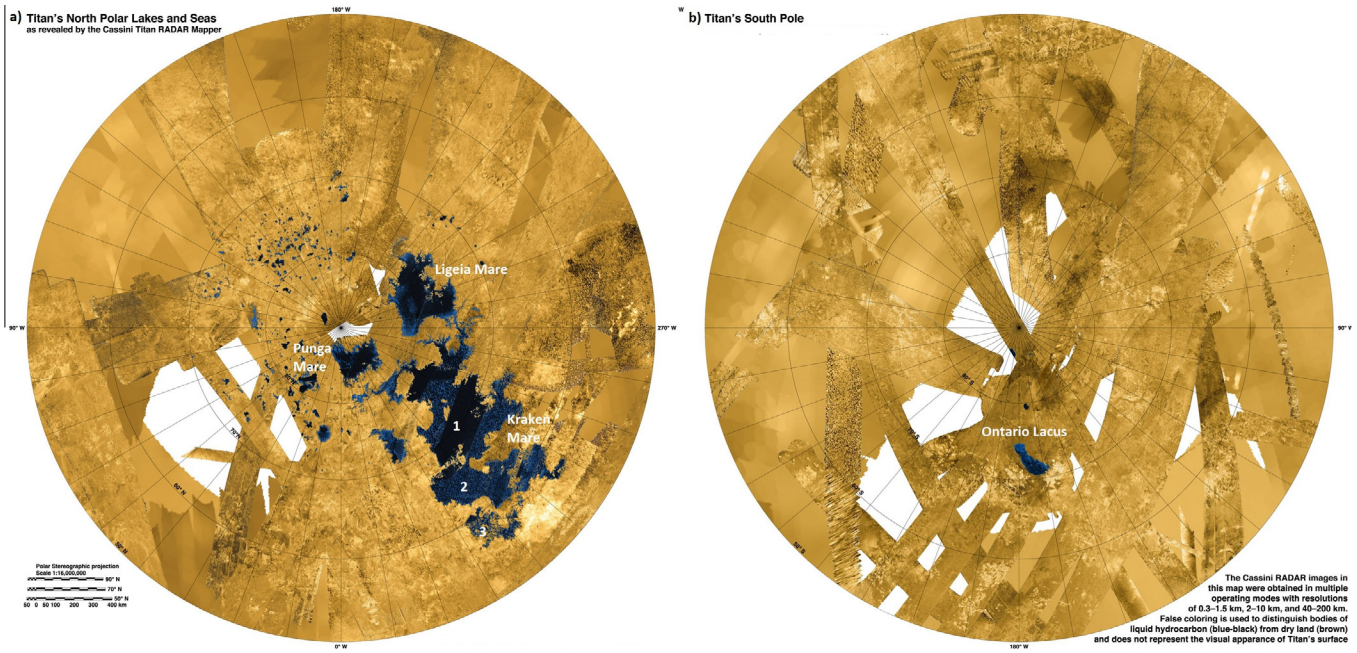


Fig. 2. Cassini radar mosaics of Titan's north (a) and south (b) polar regions (stereographic projection: the color table is adjusted to portray liquid hydrocarbon areas as black and blue). The dramatic difference between liquid cover in the north and south is apparent. The three seas, Punga, Ligeia and the sprawling Kraken Mare (areas 1, 2 and 3 refer to splashdown targets in the text) and many small lakes dominate the north, while Ontario Lacus offers the only prospective target in the south. White areas are unimaged by radar at present. Image: NASA/JPL/USGS. (For interpretation of the references to color in this figure legend, the reader is referred to the web version of this article.)

tidal dynamics – Tokano et al., 2014). One region ('Kraken-1') is the largest dark area observed in the near-IR, and was also imaged by the Cassini radar on flyby T30 in 2007 and on T91–95 in 2013, and is centered at 70°N 315°W: its radar reflectivity is generally at the noise floor of the instrument, suggesting that Kraken, like Ligeia, is deep. Ligeia Mare was measured to have a depth of 160 m, using radar altimetry in 2013 (Mastrogiuseppe et al., 2014) A second area, further south (and thus permitting a later mission) is centered at 64°N, 320°W. Finally, we consider Ontario Lacus in the south (71.6°S, 186.6°W). We discount unconfirmed reports of low-latitude lakes: even if such features are real, they are likely to be shallow and probably transient and thus are unreliable targets on which to base mission planning. Indeed, other low-latitude locations on Titan have been observed (Turtle et al., 2011a,b) to darken following cloud activity, and then subsequently brighten (presumably as a result of evaporation of shallow surface liquids).

We evaluate the tolerable landing point dispersions (i.e. we define the largest ellipse which is completely – 99% – within the margins of the sea) for each of these locations using a Monte Carlo method as follows. Offsets from a nominal target location are assumed to be normally-distributed (i.e. Gaussian) in kilometers, in both the zonal and meridional directions, with the zonal dispersion typically the larger. From 1000 such points, the number that fall within the apparent bounds of the dark area is calculated by looking up the image intensity at the corresponding pixel and reporting a successful splashdown if the intensity is below a threshold of about 10% of the peak brightness in the mosaic. Some example footprints are shown in Fig. 3 (for Kraken-1) and Fig. 4 (for Kraken-2 and Ontario). 1000 or more instantiations are required in order to reliably count 'misses': for a 99% ellipse – where the major axis corresponds to 5 times the standard deviation specified in the zonal direction – about 10 cases will fall on land.

For Kraken-1, about 1% of instances of a dispersion calculation fall on land when the standard deviations in the zonal and meridional directions are 90 km and 18 km respectively, i.e. a 450 × 90 km 99% ellipse. If a more aggressive risk posture is adopted, such that 1 in 20 cases miss the sea, the allowable ellipse becomes 500 × 250 km or 575 × 100 km. Clearly, the size of ellipse one can choose for an acceptable miss probability depends on the location chosen, and on the orientation of the ellipse, which will depend on the specifics of the entry angle, approach azimuth, descent time and the winds. For worlds with dense atmospheres (Titan, Venus), the landing point uncertainty is typically dominated by the zonal winds (Lorenz, 2015) and so an E–W aligned ellipse is a useful metric. Note that in Kraken as a whole, an almost circular ellipse could be accommodated, were it not for the islands in the middle, which force the N–S axis to be rather smaller.

A tolerable ellipse for Ligeia Mare is of the order of 300 × 130 km whereas for comparison, the estimated 99% landing ellipse of the TiME mission at Ligeia in 2023 was

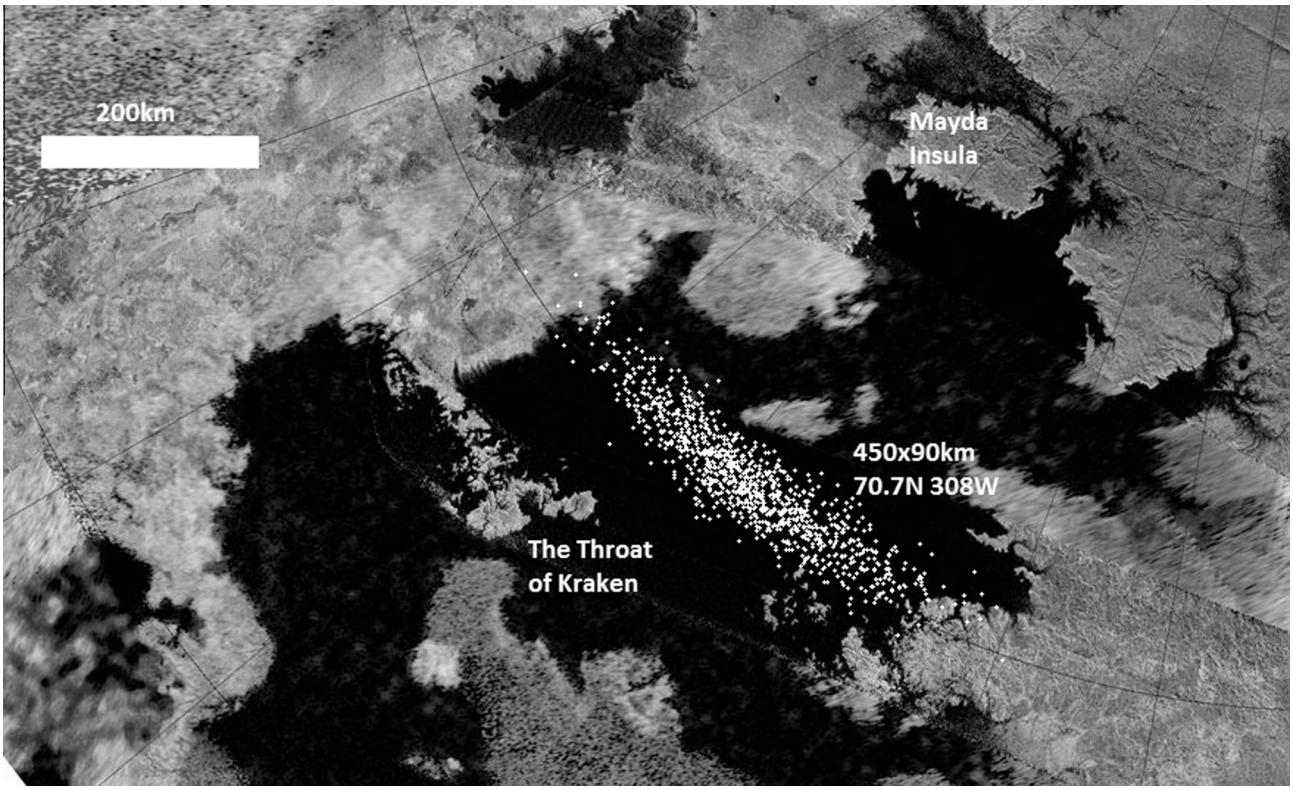


Fig. 3. Splashdown ellipse centered on 'Kraken-1' at 70.7°N, 308°W, overlain on a Cassini radar mosaic. A '99%' dispersion of 450 × 90 km can be accommodated – in this instantiation, 12 of the 1000 instantiations hit land.

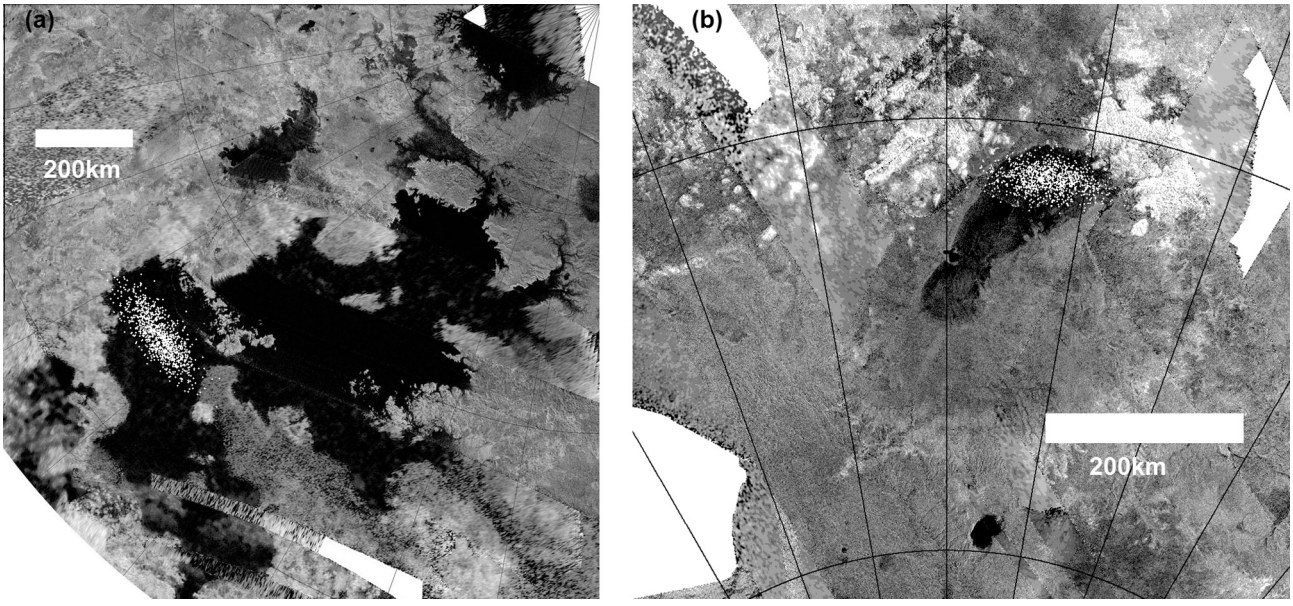


Fig. 4. Example dispersions for (a) Kraken-2 – here a 99% 270 × 100 km ellipse centered at 64.5°N, 37°W and (b) Ontario Lacus – note the change in map scale. The ellipse here, 160 × 60 km, sees some 6.7% of cases fall on land. A smaller 80 × 60 km ellipse would achieve the 99% criterion typically considered.

of the order of 110 × 110 km (see Stofan et al. (2013)). Punga Mare allows only a ~120 × 120 km ellipse, or ~190 × 70 km if oriented ideally. The upper part of Kraken Mare, near Mayda Insula, allows ~210 × 190 km centered at about 75°N, 300°W.

The basin labeled Kraken-2 is rather smaller than Kraken-1, although fortunately has its longest dimension in the zonal direction, where dispersions are expected to be largest: 99% delivery ellipse to 65°N 324°W is 210 × 100 km. A final region at ~60°, designated

'Kraken-3' in Fig. 2, may or not have liquid of adequate areal fraction or extent to be viable – further remote sensing data is needed to determine this.

The only significant body of liquid in Titan's southern hemisphere at the present day is Ontario Lacus (e.g. Turtle et al., 2009, 2011a,b; Wall et al., 2010; Cornet et al., 2012a,b). The fact that it is merely a 'Lacus' rather than a 'Mare' attests to a qualitative distinction between it and Kraken and Ligeia – not only is it somewhat limited in horizontal extent, but there is some evidence that it is rather shallow (Hayes et al., 2010), rather muddy (Clark et al., 2010), and quite possibly shrinking as Cassini has observed (Turtle et al., 2011a,b; Hayes et al., 2011). A 'bathtub ring' of brighter surface material, possibly evaporite deposits (Barnes et al., 2011) suggests a longer-term drop in liquid level, that may be consistent with the seasonal asymmetry (Aharonson et al., 2009) with southern summer shorter but more intense than the north, resulting in a transfer of volatiles to the north. Thus any mission to Ontario must presently confront the possibility that it may land in shallow liquid, and quite possibly sticky or muddy liquid, and that even areas that are liquid-covered at present may not remain so some years hence. On the other hand, other workers contend (e.g. Cornet et al. (2012a,b)) that no retreat has occurred 2004–2009 and it is possible that unexpected transparency of the liquid means the non-zero radar reflectivity arises from comfortable depths. Ontario, 250 km long by roughly 70 km wide, is inconveniently aligned approximately north–south (see Fig. 4): a 99% delivery ellipse aimed at its widest part is only $\sim 100 \times 50$ km or $80 \times 60$ km.

### 2.2. Seasonal change of communication geometry

A mission using a relay spacecraft either in orbit around Titan or even around Saturn (as was proposed in the TSSM study (ESA, 2009) can be conducted on any of the Titan seas at any time. However, multiple elements raise mission cost and complexity, and so the possibility Direct-to-Earth (DTE) communication is an important consideration. Since the sub-Earth and sub-solar latitudes are always within a couple of degrees of each other, it follows that those locations/seasons when Earth is visible are also those where the sun is above the horizon, although extended periods of twilight may allow some imaging science when DTE is not possible (nautical twilight on Earth corresponds to a sun elevation of $-6^{\circ}$). The evolution of the sub-Earth latitude in the 2020s is shown in Fig. 5.

Although of only modest importance for both meteorology and communications, it may be noted that Titan's distance from the sun decreases systematically through the 2020s, from 10.03 AU in 2020 (aphelion is in 2018, just after northern summer solstice) through perihelion (9.01 AU) in 2032, allowing a 20% increase in data transmission. The distance then increases and link performance declines again.

### 2.3. Communications and science return

As noted by Lorenz (2000), it is possible to equate, at least crudely, the data return from an in situ mission at Titan in bits to its installed energy capacity in Joules, i.e. 1 bit of science data costs 1 joule to acquire and send. This rule of thumb may be inaccurate in missions optimized for high data volume but is a useful starting point for typical in situ vehicles. To a first order, then, it is unimportant whether 10 Mbit of data are sent at 3 kbit/s over one hour, or at 100 bit/s over 30 h – the total energy requirement is 10 MJ (or 3 kW-hr) in each case. However, if electrical power is continuously generated (e.g. from a radioisotope power source) then the overall strategy of data return, dictated by Earth visibility, may result in energy being discarded unless massive battery storage is provided.

Thus the 'ideal' scenario for a polar mission, from a telecommunications and power standpoint, is one at the highest latitude (i.e. Ligeia) at the peak of summer ('midnight sun') where the Earth never actually sets, and thus communications can be performed continuously and data are transmitted as they are acquired at a rate that is matched to the electrical power available. In such a scenario, with 100 W of electrical power available for telecom, a vehicle could transmit 100 bps continuously, and therefore provide a data return over 1 Titan day (15.945 Earth days, or $1.38 \times 10^6$ s) of almost 150 Mbit, roughly the equivalent of the return from the Huygens probe.

As we move away from the pole, the Earth and sun take a progressively more inclined path across the sky. The fact that Earth reaches a higher elevation is not fundamentally significant, since atmospheric path loss will not be severe for X-band or lower frequencies anyway. What becomes critical is for how long the Earth is high enough to permit communication.

When the Earth is only above the permitted elevation threshold for a small fraction of a Titan day e.g. 2 Earth days, we can imagine attempting to return the full data amount indicated above (150 Mbit) in that time. This would require a data rate of nearly 900 bps, and thus a power of around 900 W. The vehicle must now have a more powerful transmitter (which may not only imposes severe hardware demands, but will also introduce more severe thermal challenges.) More challenging yet is the energy storage requirement – while in each Titan day the primary power source (the radioisotope generator, supplying 100 W) can indeed provide the energy per Titan day to accomplish the 150 Mbit transmission, a battery must supply 800 W (=900 W–100 W) for two earth days, i.e. an energy storage of some 38 kW-hr. If we assume a typical modern energy density for high-performance *rechargeable* lithium batteries of 100 W-hr/kg, this would entail a somewhat impractical 380 kg of battery. In other words, for the scenario when the Earth is visible for only part of the day, the time-averaged data rate becomes storage-limited rather than power-limited. Or put another way, without very large

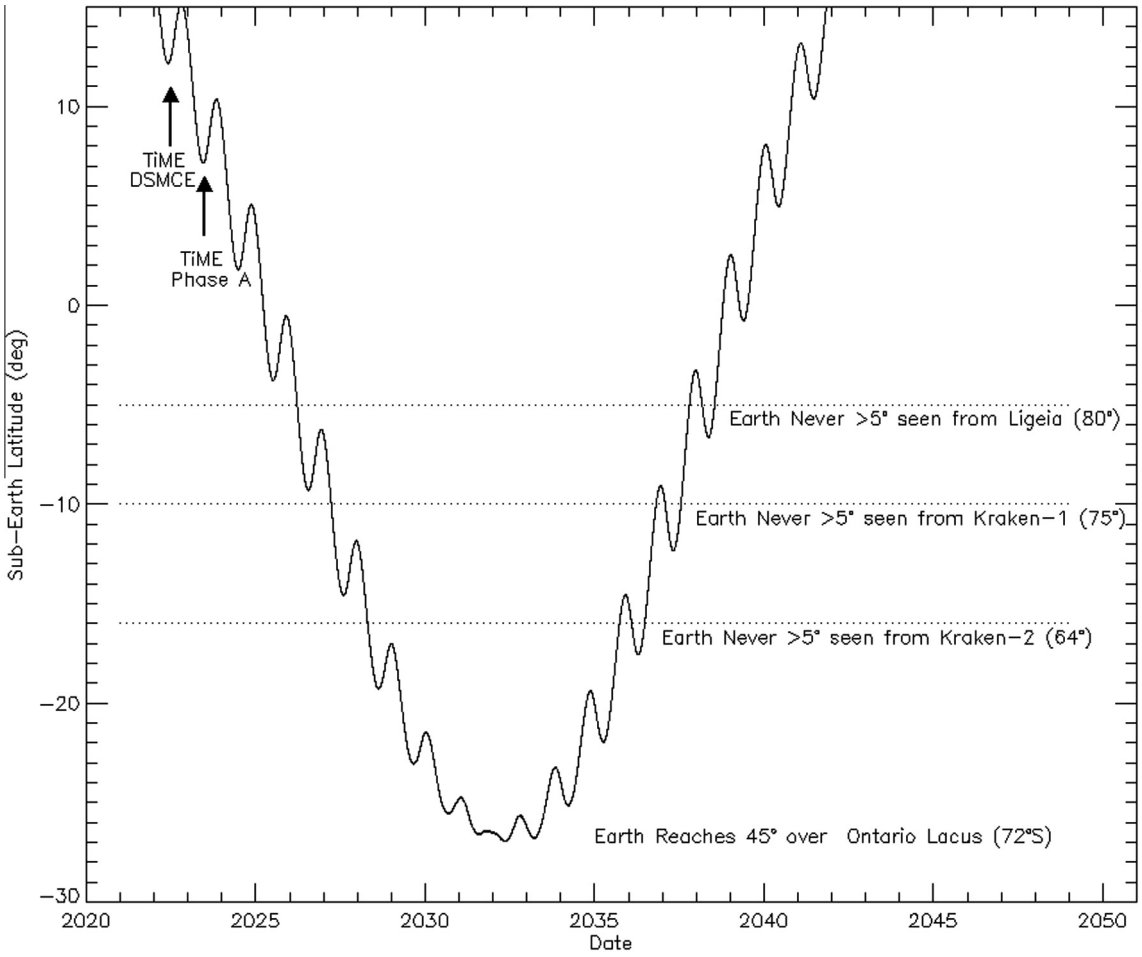


Fig. 5. Direct-to-Earth communication and tracking opportunities depend on the sub-Earth latitude which changes most rapidly around equinox in 2025: a $\pm 2^{o}$ superposed annual oscillation is due to the Earth's motion around the sun. As solstice is approached in 2032 the movement slows. Ontario Lacus in the south is visible throughout the period shown.

on-board energy storage, the data return becomes directly limited by the number of hours per Titan day that the Earth is visible above some threshold elevation.

We show, therefore, this metric in Fig. 6, with a conservative elevation threshold of $10^{o}$. Depending on the sea state and the antenna beam pattern, such an elevation should be relatively free of multipath effects (which were observed in the Huygens telemetry link to Cassini, Pérez-Ayúcar et al., 2006) or atmospheric attenuation. Furthermore, only pathological shoreline topography (i.e. north-facing cliffs) can therefore obstruct Earth view near the edge of the seas: even 300 m high mountains could only block a $10^{o}$ line-of-sight out to 2 km. Also shown are the visible hours per day for an elevation mask of $5^{o}$, which should be viable for communication on the open sea, but suffers more atmospheric effects (refraction and attenuation), and a higher probability of terrain blockage and/or multipath effects.

One may note that since a floating vehicle may drift tens of km per Titan day in response to surface winds (Lorenz et al., 2012b) the vehicle's latitude could change by about a degree in this period, and the maximum Earth elevation change by a similar amount. Thus Fig. 6 could be reasonably interpreted as follows: for a given acceptable hours-per-Titan day of visibility, the solid curve ($10^{o}$) corresponds to when one can be reasonably assured of maintaining communications for one or more Titan days, whereas the dashed ($5^{o}$) curve denotes when significant risks of at least sporadic communication loss may occur after 1 Titan day.

A 100-h threshold might be adopted as a defendable 'round number' for a balanced science mission – in 1 Titan day a data return of $100 \times 3600 \times 100 = 36$ Mbit should be achievable, or a Huygens-like return in 4 Titan days. One can of course propose lower or higher thresholds – a mission performing only meteorological measurements like a terrestrial weather buoy without much imaging data could be achieved with over an order of magnitude less data, for example. We reiterate also that a mission equipped with a relay spacecraft need not be constrained by Earth visibility, although such a mission could be enhanced by DTE radio science.

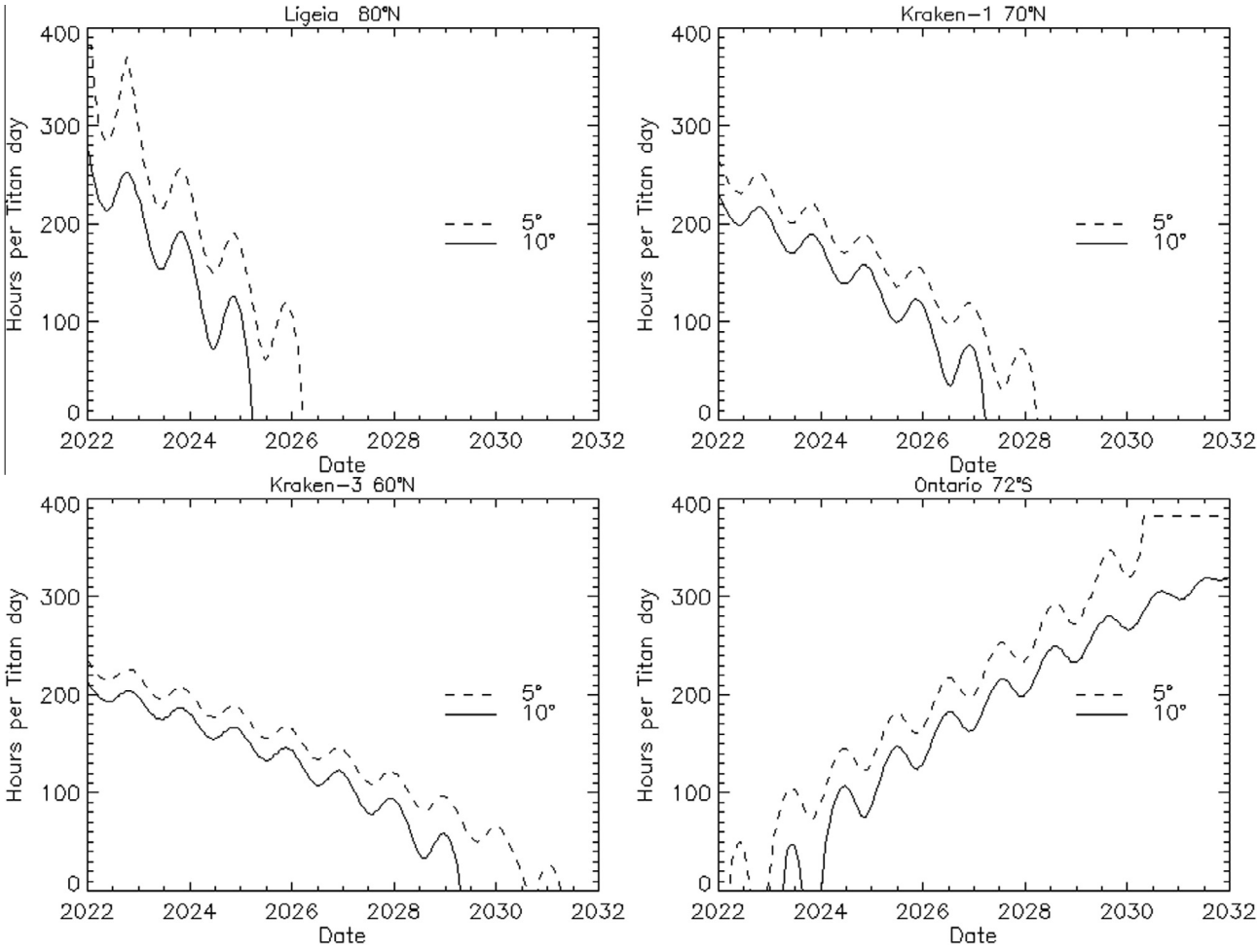


Fig. 6. The Earth hours per Titan day that the Earth is above some specified elevation threshold (5° or 10°) as seen from each location. The rapid decline in visibility from Ligeia ((a), the northernmost site) is especially evident – a robust (100 hr @ 10°) mission is possible until 2025 at the latest. Sites further south (Kraken-1 and -3) have slower declines as one might expect, being viable until 2026 and 2027 respectively. Ontario Lacus becomes viable around 2025 and progressively improves, having uninterrupted Earth view after 2030.5.

## 3. Wind variations with latitude and season

Having first considered possible splashdown locations, and their visibility from Earth, we now turn to when (or indeed whether) these sites can be safely reached. As noted during the development of Huygens (which had no requirement to land at a specific location), the low gravity and high density of the Titan atmosphere leads to low descent speeds, and the large scale height means parachute descents begin at high altitude. These effects lead to long descent times (>2 h) which give the zonal winds time to sweep a descending vehicle eastwards (e.g. Flasar et al., 1997), plus some stochastic drift in any direction. This dependence of landing dispersion on rather imperfectly-known environmental characteristics presents the designer of new missions, aimed at specific targets, with interesting challenges. Before evaluating landing dispersions in detail in Section 4, we first review how the descent wind environment changes at different latitudes and seasons.

### 3.1. Zonal winds in Global Circulation Models

As discussed in Friedson et al. (2009), a key discriminator among Titan GCMs appears to be the extent to which they predict the zonal superrotation (see also Lorenz et al. (2012a)). Typically, GCMs have tended to greatly underpredict the stratospheric superrotation, although some of the latest models show better success in this respect, with TitanWRF (Titan Weather Research and Forecasting, Richardson et al. (2007), Newman et al. (2011)) and the IPSL model (Institut Pierre Simon Laplace, Lebonnois et al. (2012), Charnay and Lebonnois (2012)) predicting superrotation magnitudes similar to those observed. The details of the altitudes at which the peak winds are encountered, and their seasonal variation, vary from model to model, however. Newman et al. (2011) found that the production of eddies which are key to the generation of superrotation is be highly sensitive to the amount of dissipation in the model dynamics,

and is prevented when horizontal diffusion within the model (included to parameterize sub-grid scale mixing processes) is too large. They obtained most realistic results when little or no explicit horizontal diffusion of angular momentum or temperature was included (though, as with most grid point models, TitanWRF also contains a small amount of implicit diffusion in its solver). The results shown here come from a 'dry' version of TitanWRF (i.e. with no methane cycle or associated latent heating effects included) and the simulation was performed assuming a flat, homogeneous surface with no lakes but including the diurnal cycle of solar forcing and the impact of gravitational tides.

In this paper, we report details from the TitanWRF model only. Of presently-published models, TitanWRF produces the strongest superrotation, and while it does predict somewhat faster zonal wind speeds in the lower stratosphere near the equator than were observed by the Huygens probe (Bird et al., 2005; Folkner et al., 2006) it offers the best agreement with thermal infrared observations by Cassini (Achterberg et al., 2011) which indicate in 2005 ($L_s \sim 310^o$) winds at the 10 mbar level (~100 km) of ~40 m/s at 60°N and at 2 mbar (~150 km) of 100 m/s at the same latitude. In addition, a further indication of the high latitude jet is that zonal winds are strong enough to distort the pressure surfaces of the atmosphere to a degree that can be detectable in the shape of the central flash of stellar occultations. Sicardy et al. (2006) infer a zonal windspeed of ~200 m/s at 55°N at $L_s \sim 290^o$ at an altitude of 250 km (0.25 mbar) in a pair of stellar occultations in 2003.

Fig. 7 shows zonal wind profiles for several sea targets in the coming decades. We see two principal trends in the model results (Fig. 7), which might be predicted from the overall behavior of thermally-driven stratospheric winds (e.g. Flasar et al. (2005, 2009)). The first is that in general zonal winds are weaker at high latitude (infinite shear at the pole would be encountered if they did not decline with latitude) – thus the Kraken winds are stronger than those over Ligeia, and the Kraken-2 winds are stronger than Kraken-1 (which resemble Ontario's, but phase-shifted by a half Titan year).

The second effect is that a strong circumpolar jet develops in the winter hemisphere. This is a general characteristic of planetary atmospheres and is seen on Earth and Mars as well as Titan (Achterberg et al., 2011; Flasar et al., 2009). Thus moving away from northern summer into fall, we expect northern hemisphere winds to freshen. This trend is seen very well in the time series for 70°N (Fig. 8) which shows TitanWRF zonal wind output every 3 Titan hours over Kraken-1, and shows that winds at progressively lower levels in the atmosphere respond progressively slower (longer lag) to the seasonal forcing. Of particular relevance to the problem at hand is that these northern hemisphere winds freshen throughout the 2020s ($L_s \sim 150^o$–$220^o$).

### 3.2. Meridional winds

Meridional winds on Titan were discussed in Lorenz et al. (2012a), which proposed a symmetric specification with a 99% envelope that increases modestly with altitude, specifically $|v| < 1 + 3(z/300)^{0.5}$, where $v$ is in m/s and $z$ in km. That specification conservatively spanned the meridional winds encountered by the Huygens probe as well as GCM results pertaining to Ligeia Mare in 2023 ($L_s \sim 160^o$). It is seen (Fig. 9) that the same specification appears to satisfactorily embrace (with minor local excursions, compensated elsewhere) the expected winds for further south, and can thus be adopted without modification for mission analysis purposes everywhere.

## 4. Landing dispersions

The landing dispersions of planetary probes depend on three major contributions, see e.g. Lorenz (2015): a delivery uncertainty due to interplanetary navigation errors (including ephemeris uncertainties in the target body itself), an entry error due to atmospheric density variations and aerodynamic effects such as body lift, and dispersions due to displacement by wind during a parachute descent. The second term is small, except for very shallow entries typical for Mars. Thus at Titan with a much thicker atmosphere where entries tend to be rather steep, and descents rather long, the last (wind) term dominates in the zonal direction due to the superrotating atmosphere. In the meridional direction, delivery uncertainties and wind displacements may be comparable.

### 4.1. Delivery errors

To a first order, an interplanetary delivery uncertainty may be of the order of a few to ~30 km, depending (e.g. Haw (2003)) on whether the last tracking information prior to release of the entry vehicle is a few days to ~30 days prior to entry: for reference, the Huygens delivery uncertainty was 6 × 31 km (1σ), in part due to poorly-determined Titan ephemeris at the time, now constrained by many Cassini flybys to better than 1 km. That delivery dispersion is 'smeared' by projection onto the spherical planet, depending on the entry angle. At Mars, where descent times, and thus wind dispersions, are small and shallow entries in the thin atmosphere are needed (e.g. Phoenix, −13°), landing ellipses are dominated by this effect, especially for high latitude targets. The thick Titan atmosphere, however, allows much steeper entries (e.g. Huygens, −65°) and thus the dispersion at the top of the atmosphere may be roughly doubled (1/sin(65°)) in the along-track direction – i.e. if the incoming asymptote is northwards and the dispersion circle in the plane normal to the asymptote (the 'B-plane') has a 99% diameter of 10 km, then the delivery points to the top of the atmosphere will be distributed in a 20 × 10 km ellipse aligned north–south.

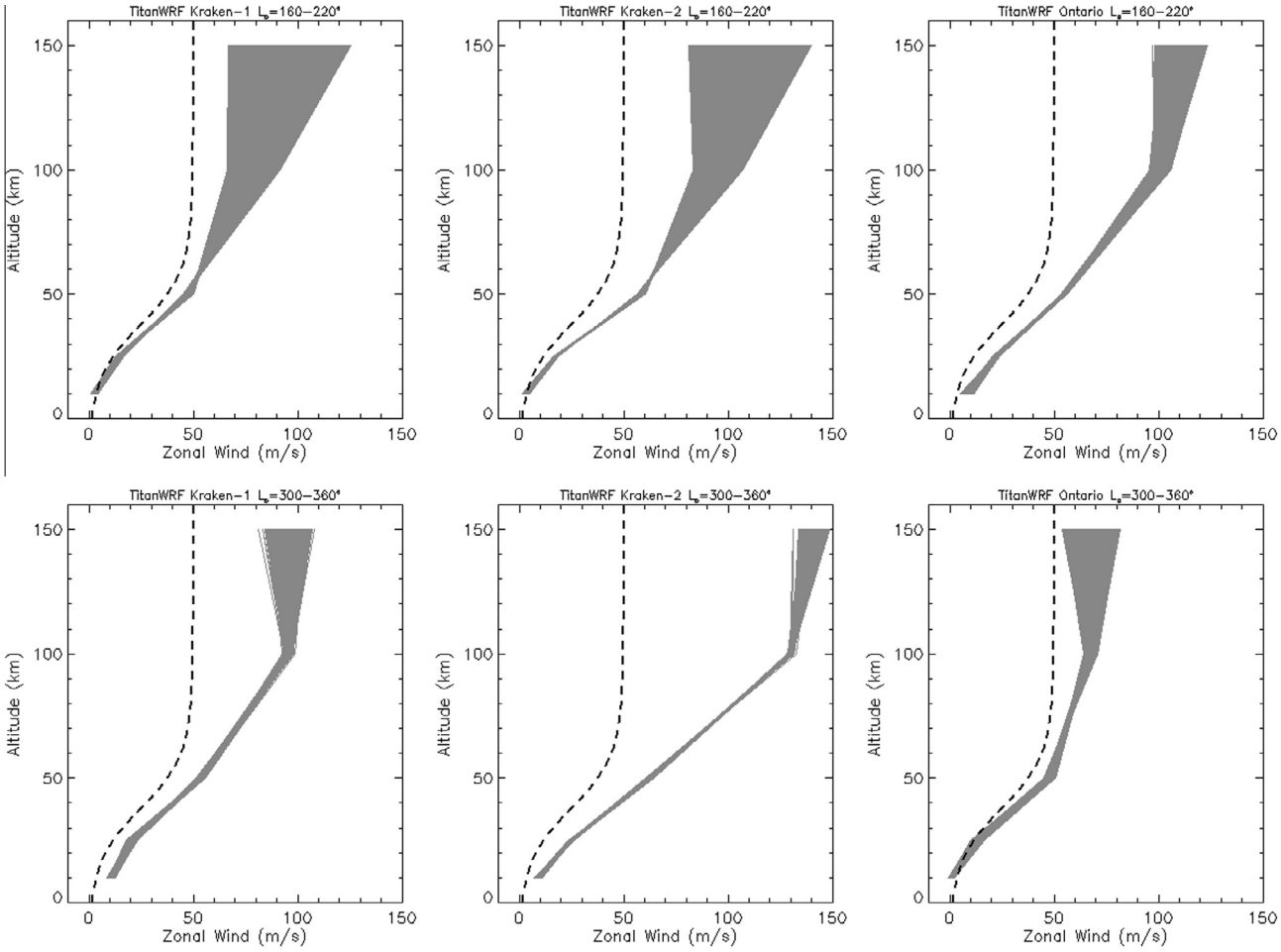


Fig. 7. Zonal wind profiles from the TitanWRF model for three locations and target locations, shown as gray triangles. The gray region shows the variation in the period shown (one sixth of a Titan year, centered around the late 2020's, $L_s \sim 190^o$, and the mid-2030's, $L_s \sim 330^o$). The dashed line is the maximum model wind profile assumed for Ligeia Mare in 2023 (Lorenz et al., 2012a) as a common reference. It is seen that the more equatorward Kraken-2 site (middle) has stronger winds than Kraken-1 (left). Note that while the winds at $L_s \sim 330^o$ have strengthened over Kraken, they are steadier – the gray region is rather narrow. Ontario Lacus at $L_s \sim 190^o$ has rather strong winds, but these calm significantly in the 2030s.

Note that because performance of heat shields is often a critical consideration for entry systems, and the aerothermodynamic loads are a strong function of entry angle, the delivery uncertainties are often referred in the literature in terms of an entry angle uncertainty ($\delta\gamma$). For steep entries typical for Titan, this may be approximately related to the position uncertainty $\delta x$ as $\delta\gamma \sim \delta x/[(R+h)]$, where $R$ is the planetary radius and $h$ the height of the entry interface, ~2575 km and ~1270 km respectively, the latter for historical reasons. The 2003 NASA aerocapture systems study (taking into account an assumed improvement in Titan ephemeris due to Cassini, but a progressive degradation thereof after 2017) anticipated a $3\sigma$ $\delta\gamma$ of $1.9^o$ after a release 30 days prior to entry, whereas an aerocapture orbiter vehicle with its trajectory guided until 2 days before entry would have $\delta\gamma$ of $\sim 0.6^o$ (Haw, 2003): the total probe and orbiter delivery uncertainties $\delta x$ are therefore ($3\sigma$) about 100 and 35 km, respectively. These values are useful working values to assume for the present exercise.

### 4.2. Wind drift

In determining the landing footprint of a spacecraft, the horizontal displacement $D$ of the landing point from the start of descent is the result of the convolution of the wind profile with the time spent at each altitude. In effect, the displacement is a weighted average of the wind profile: for a single parachute, the weighting function can be simply approximated (Lorenz et al., 2012a; Lorenz 2015) by the square root of atmospheric density $\rho$ at each altitude. Here we estimate the sum $\Sigma\rho^{0.5}(z)U(z)$ for $z = [10, 25, 50, 100, 150]$ km. For the nominal 2023 Ligeia wind profile in Lorenz et al. (2012a) with a single parachute descent from ~150 km, this sum yields 27 $\mathrm{kg^{0.5}\,m^{-0.5}\,s^{-1}}$, corresponding to an *expected* 75 km displacement for a vehicle with a descent time of 8900 s (that of the Huygens probe). Thus, a simple prefactor of 2.8 $\mathrm{km/kg^{0.5}\,m^{-0.5}\,s^{-1}}$ can more generally convert the sum into the expected displacement at other locations and seasons – the prefactor

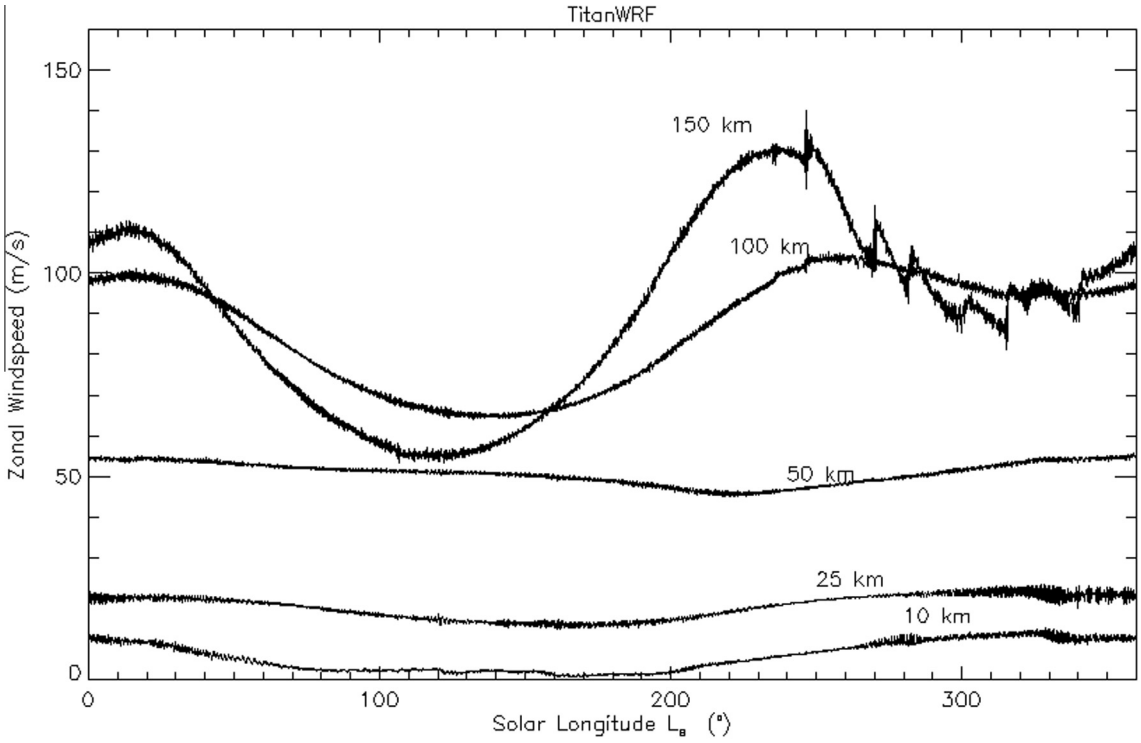


Fig. 8. Seasonal history of zonal winds at 70°N for five altitude levels in the TitanWRF model. Winds increase monotonically with altitude except for a brief period in the stratosphere in northern summer ($L_s = 40°$–$140°$). The seasonal modulation is significant in the stratosphere, and declines at deeper levels, where it also becomes phase-lagged with respect to the solar forcing (the minimum speed at 150 km occurs at $L_s = 110°$, about 1.5 Earth years after summer solstice, whereas the minimum at 50 km altitude is almost a Titan season later). The sharp spikes in the 150 km profile are momentum transfer events, discussed in Newman et al. (2011).

would be different for other vehicles/parachutes, and proportional to the total descent time.

The *dispersion* in landing points will scale with the difference between the estimate for the minimum and maximum winds, in the Ligeia case, 209 km E–W (−30 km to +175 km – Lorenz et al., 2012a, Fig. 3), interpreted as a 99% range (or $\sigma \sim 40$ km for a symmetric Gaussian). While one might, in a full mission design exercise, conduct a Monte Carlo simulation of entry points, variable vehicle parameters, and varying wind and atmospheric density profiles, to a first order the landing point dispersion is dominated by the winds, and so a normally-distributed set of landing point offsets can be applied in the zonal and meridional directions. In this case, the standard deviation to be applied in the zonal direction will be one fifth of this range (99% corresponds to ~2.5σ). This now allows us to map the zonal wind predictions to the splashdown dispersions.

Fig. 10 shows the *expected* zonal displacement as a function of season and location using the TitanWRF predictions. It is seen at once that Kraken-1 displacements in 2025–2027 are ~150–170 km, which are rather larger than the ~35 km delivery error noted in the previous selection.

An important question is how to relate the dispersion to the expected values above. As noted in Lorenz et al. (2012a), TitanWRF predictions (see the Ligeia 2023 datapoint in Fig. 10 showing the expected displacement of 120 km in 2023) were about 50% higher than the average of various models and observations, and about 60% of the range (209 km) between minimum and maximum models. Thus conservatively we might assign the same factor (~1.75) to scale up the TitanWRF expected value to the 99% range. It is possible in future that additional observations may allow the narrowing of this factor, but at present GCMs are sufficiently discrepant and data sufficiently sparse (especially in the troposphere, where a descending probe spends most of its time) that it is difficult to justify dismissing any individual model.

Applying this factor, then we find Kraken-1 zonal dispersions of ~1.75*160 = 280 km in 2025–2027, but growing to some 440 km in the 2030s, with Kraken-2 dispersions varying between 315 and 490 km. Ontario dispersions vary, depending on season, between 215 and 440 km. The meridional wind envelope shown in Fig. 9 correspond to 20 km descent dispersions – we use this value for all places and seasons.

### 4.3. Final dispersions

We can derive estimates of the final landing ellipses by root-sum-squaring the delivery dispersions in the zonal

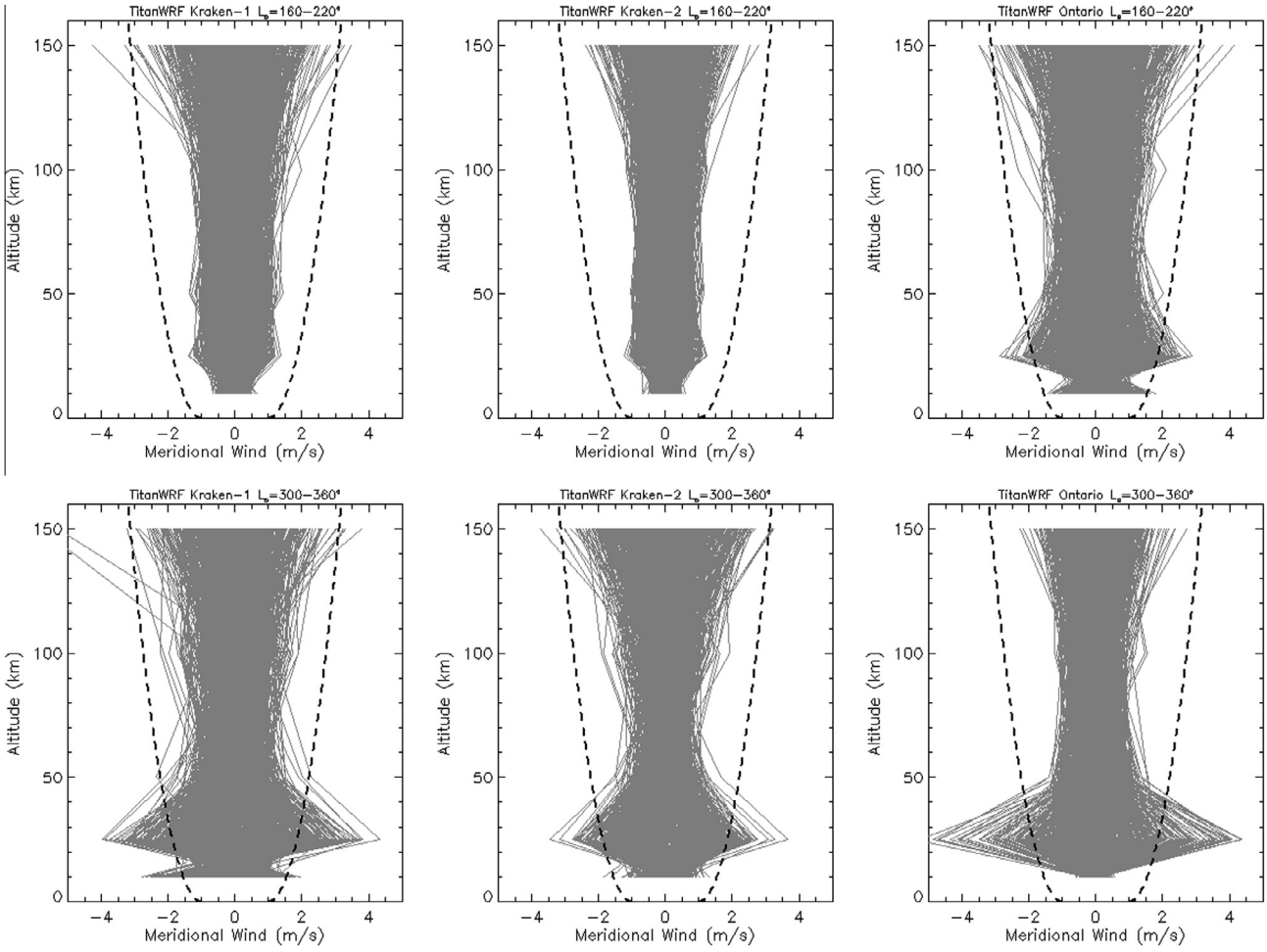


Fig. 9. Meridional winds (m/s) in the TitanWRF model for the Kraken-1and -2, and Ontario target region (the 'tornado' of narrow lines) together with a general meridional wind envelope (see text) from Lorenz et al. (2012a), thick dashed curves.

and meridional directions with the wind dispersions. If we assume the 35 km delivery (~99%) uncertainty indicated above for a 2-day navigation solution, an entry angle ($-60^{o}$) similar to Huygens and a north–south asymptote, then the top-of-atmosphere delivery ellipse is $35 \times 70$ km. The meridional winds smear these points north–south by a maximum of 20 km, and thus the north–south dimension of the landing points is $(20^2 + 70^2)^{0.5} \sim 72$ km. Taking Kraken-1 in the 2030s as an example, with a zonal wind dispersion of 300 km, the long axis of the final ellipse will be $(300^2 + 35^2)^{0.5} \sim 302$ km, and thus the landing points are within a $302 \times 72$ km ellipse, comfortably within the safe area ($450 \times 90$ km). For comparison, were the delivery asymptote aligned E–W, the resultant ellipse would be $308 \times 40$ km. Similarly, for a probe released some distance from Titan (e.g. 30 days prior to encounter), a 100 km delivery uncertainty would lead to a splashdown ellipse of $316 \times 200$ km or $360 \times 102$ km. Clearly, the viability of any given target will depend on the specifics of the entry angle, dispersion and azimuth as well as the winds, but these values provide a basis on which to eliminate unpromising mission candidates.

## 5. Summary – mission opportunities with huygens descent systems

We summarize the results of these calculations in Table 1. First, Kraken-1 appears to be large enough that it is always accessible for well-navigated deliveries ($dx \sim 35$ km). Even for release tens of days out ($dx \sim 100$ km) the dispersions are small enough that detailed analysis can probably show the $450 \times 90$ km ellipse can be targeted, unless the entry angle is shallow and the delivery asymptote is north–south.

If we assume Ligeia descent displacements are proportional to Kraken-1 values (in the same proportion as the 2023 results in Fig. 10), then Ligeia is large enough for a high probability of successful splashdown at all seasons (although unfortunately its window of DTE visibility ends the soonest.)

Kraken-2 appears marginal. The smallest zonal wind dispersion of 315 km is larger than the allowed ellipse size, even ignoring the contribution from delivery errors. It is possible that additional data to refine wind dispersion models could allow Kraken-2 to become viable, but it will

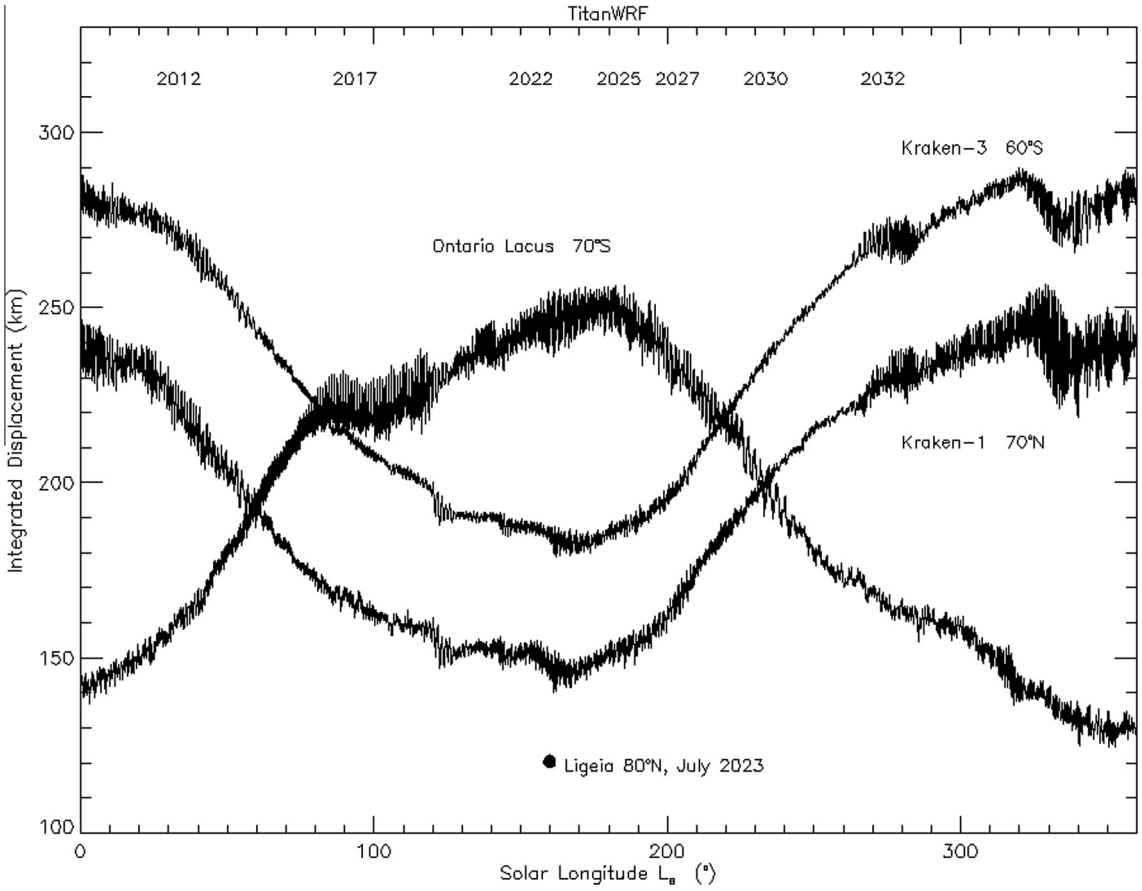


Fig. 10. The integrated displacement (summed TitanWRF zonal wind speed times square root of density at 10, 25, 50, 100 and 150 km) for the three targets of the late 2020s. The point for Ligeia Mare indicating the proposed TiME mission in 2023, based on the TitanWRF profile in Lorenz et al. (2012a) is also shown. It is evident that the displacement increases systematically equatorward. From about 2015–2027, the winter stratospheric jet over Ontario Lacus causes that target to have larger displacements even than the most equatorial Kraken target. Kraken target dispersions increase by about 10% per year over the 2025–2032 timeframe, leveling out over winter. Only in late southern summer does the displacement for Ontario become comparable with that of Ligeia in 2023.

Table 1
Targets, allowable dispersions, visibility and delivery opportunities.

| Splashdown site | Target | Ellipse (99% E–W, N–S) | DTE window (>100 h/Tsol, >10°) | Remarks (99% accessibility with Huygens descent time) |
|---|---|---|---|---|
| Ligeia | 78°N 245°W | 300 × 120 km | <2024, >2040 | Almost always accessible unless meridional delivery errors large |
| Kraken-1 | 70.7°N 308°W | 450 × 90 km or 240 × 200 km | <2026, >2038 | Always accessible (e.g. 302 × 72 km in the 2030s) unless meridional delivery errors large |
| Kraken-2 | 65°N 324°W | 270 × 100 km | <2027, >2037 | Zonal dispersions always just (315 km) too large? |
| Ontario | 72°S 178°W | 80 × 60 km | 2025–2040 | Zonal dispersions always too large (>100 km) |

only be so for a modest period during winter when the stratospheric winds are weaker.

Ontario appears hopeless for passive parachute delivery. It is simply too narrow in the E-W direction to accommodate any reasonable wind dispersion – the 90 km allowed width is a factor of more than two smaller than the wind dispersion, and delivery uncertainties exacerbate the problem. For a long-range delivery (tens of days release) the entry dispersions alone make it difficult to be sure of landing in liquid.

Note that there has been progress in this arena. The first post-Cassini lander design was that of the 2007 Titan Explorer Flagship mission (Leary et al., 2007; Lockwood et al., 2008) which featured a lander. At the time, the seas had only just been discovered, and the (airbag-equipped) lander was aimed at the equatorial dunefields, these being a large, contiguous area that would not present significant boulder or gully terrain hazards. Landing dispersions (a 720 × 220 km ellipse) were estimated with a model (Titan-GRAM, developed pre-Cassini) which is now known (Lorenz et al., 2012a) to grossly overpredict meridional dispersions. That version of Titan-GRAM also fails to include any systematic variation of zonal wind speed with latitude and season, which we show here are

important but somewhat predictable. The delivery ellipses discussed in this paper allow for much tighter targeting than was the case seven years ago.

## 6. Mission and spacecraft design alternatives

The discussions in this paper have been with reference to a somewhat arbitrary 99% success criterion, typical of single-spacecraft missions. One can of course entertain a higher level of risk, e.g. if a mission were to be considered partly successful if it landed near the shore, although the probability of survival is much harder to estimate given our ignorance of small-scale topography on Titan. Another mission-level approach is to deliver multiple vehicles, and allow that some may fail, but that objectives are achieved if one lands successfully in the sea.

The wind dispersions, which dominate the discussion, apply to a Huygens-like descent, lasting 8900 s and starting from 150 km altitude. One could vary a number of mission parameters to reduce this dispersion – e.g. a higher entry ballistic coefficient (higher mass/area) would penetrate deeper into the atmosphere, allowing a shorter descent, albeit at the cost of more demanding heat loads during entry. A similar result, with a similar penalty in heating, results from a faster entry speed, or a steeper entry. However, as an example, doubling the entry speed, with an almost order-of-magnitude increase in peak heating rate, will penetrate only about half a scale height deeper into the atmosphere (say ~20 km), reducing the zonal dispersion (see e.g. Fig. 3 of Lorenz et al. (2012a)) by only ~10 km, not enough to meaningfully alter the conclusions of this paper. A smaller descent parachute (or indeed none altogether) would allow a slightly faster descent, although possibly at the expense of attitude stability which may be important for imaging. A faster descent also leads to higher splashdown loads. There are limits in any case on how dense a capsule can be, since it must float.

It is, however, worth considering just what the landing requirements would be to splash down in Ontario Lacus, since it is prominently visible from Earth in coming decades. It is evident that such a tight splashdown area cannot be obtained by simple vertical descent (relative to the air) since it is the poorly-known movement of the air itself that dominates the landing point uncertainty. Thus the capability for controlled (i.e. guided) horizontal movement must be built into the vehicle – in other words it must fly to Titan's surface, not merely fall to it. Since aerothermodynamic loads on a Titan entry vehicle may be quite modest, it might be possible to achieve an integrated one-stage design (resembling, perhaps, the Space Shuttle or one of its predecessor lifting body test vehicles). A more conventional approach (suggested as 'Mission Concept 3 – Gliding Lander' in Lorenz (2000)) is to deploy a parawing or steerable parachute: the deployment of an inflatable/flexible ('Rogallo') wing after entry from orbit was in fact studied quite seriously for the Gemini capsules in the 1960s.

The simplest description of a system is the glide ratio or lift:drag: if a vehicle can attain a glide ratio of 3:1, then if it is released and can acquire its desired trajectory (parafoils are only able to execute slow turns, for example) at an altitude of 100 km, then it can in principle traverse a horizontal distance of 300 km. Simple steerable parachutes (circular canopies with a slot) have glide ratios of about 0.5 (e.g. Knacke, 1991; Rogallo, 1967). Since descent dispersions of the order of 160 km ($2\sigma$) must be negated, it follows that a glide ratio of ~1 or higher must be achieved.

Higher-performance, and currently operational steerable parachute systems such as the JPADS (Joint Precision Airborne Delivery System – Brown and Benney, 2005) achieve glide ratios of 3:1 to 4:1 (somewhat less than the idealized 5:1 assumed by Lorenz (2000) – note that the system as a whole with the probe and suspension lines will have a lower glide ratio than the parawing structure itself). Thus when released at 10 km in still air, they can reach targets >30 km away, and do so with accuracies of 100 m or better using GPS guidance – such systems are now routinely used to accurately deliver supplies and equipment e.g. in Afghanistan to avoid exposing the launch aircraft to ground fire. Steerable parachutes are space-qualified – one was flown in space for 3 years without degradation (Witkowski, 2010) on the Genesis capsule (although not, unfortunately, deployed).

Some detailed recent performance data is available from tests of a steerable parachute (parafoil) for the X-38 crew return vehicle (Stein et al., 2005). This parachute demonstrated L/D of ~2.8–3.4, depending on the control line position. This corresponded to a lift coefficient of 0.5–1.0.

There is one complication associated with parafoil delivery, which is that the vehicle has an appreciable horizontal velocity. Thus a parafoil flying at $L/D = 3$ and a descent rate of 5 m/s (like Huygens) will have a horizontal velocity of some 15 m/s. Such a velocity may not be safe for splashdown (some dynamic effects of horizontal motion at splashdown on the Apollo capsules are examined by Lorenz (2011)). It may be possible to 'flare' the chute or otherwise reduce the $L/D$ just prior to impact using the steering actuators, or alternatively switch to a conventional parachute at low altitude. These measures require either that the altitude above the lake surface be measured with a precision of a few meters (likely requiring a radar altimeter or similar capability) or that the vehicle switch to a more conventional parachute in the last km or two of descent (which could be triggered by inertial guidance or pressure sensing, but requires an additional parachute and release/deployment system). The targeting accuracy would be limited by the navigation/guidance capability, which while much poorer on Titan than is possible on Earth with GPS should nonetheless be adequate. For example, the inertial guidance on the Curiosity rover, Martin-Mur et al. (2012), achieved sub-km precision: even allowing for greater ephemeris errors, and larger divergence of the navigation solution during the longer descent at Titan, the center of Ontario could be comfortably reached.

## 7. Conclusions

We have considered the extent of seas on Titan, their visibility from Earth, and the likely landing dispersions due to winds. The dispersions associated with Huygens-like descent systems comfortably permit accommodation in the widest part of Kraken Mare (Kraken-1) at around 70°N, where Direct-to-Earth communications can be assured until 2026, and are likely viable with some risk until 2027. Earth visibility at Ligeia Mare is inadequate for DTE after 2024, based on a criterion of 100 h per Titan day of visibility above 10° elevation. The Titan Mare Explorer (TiME) mission was proposed in 2010, with an anticipated 2016 launch date and 2023 arrival. Now in 2015, it is too late for any realistic development schedule and interplanetary delivery to accomplish an affordable (DTE) mission to Titan's seas until summer returns to the north in 2040. Missions to Kraken-1, albeit dimly lit by low sun or twilight in Titan's hazy atmosphere, are always possible if a data relay spacecraft is available.

An additional year of Earth visibility (until 2028) is afforded from a southern basin in Kraken at 64°N, but present models suggest strong zonal winds building up in this season (the winter stratospheric jet) and suggest zonal landing dispersions too large to be viable for this location. Both the southernmost parts of Kraken (at 60°N) and Ontario Lacus have been considered, although may have shallows or mudflats that are not well-characterized by current data. Ontario sees adequate and improving visibility throughout the second half of the 2020s – but is too small to have an acceptable probability of being reached by a simple passive descent system. A guided descent using present-day steerable parachute technology could likely reach a desired target location, but with additional complexity, actuator qualification requirements, landing flare or release requirements.

While other missions to Titan remain affordable and appealing in the coming decades (for example, an orbiter, or an aircraft), the most efficient exploration of Titan's seas specifically may need to wait until 2040.

## Acknowledgments

R. Lorenz was supported for this work by the Johns Hopkins University Applied Physics Laboratory. C. Newman acknowledges the support of the NASA Outer Planets Research Program and access to the NASA Ames High End Computing facility, on which all simulations were performed. RL thanks B. Charnay, S. Lebonnois and J. Mitchell for discussions and comparisons with other model results.

## References

Achterberg, R.K., Gierasch, P.J., Conrath, B.J., Flasar, F.M., Nixon, C.A., 2011. Temporal variations of Titan's middle-atmospheric temperatures from 2004 to 2009 observed by Cassini/CIRS. Icarus 211, 686–698.

Aharonson, O., Hayes, A., Lunine, J.I., Lorenz, R.D., Elachi, C., 2009. An asymmetric distribution of lakes on Titan as a possible consequence of orbital forcing. Nat. Geosci. 2, 851–854.

Barnes, J.W., Bow, J., Schwartz, J., Brown, R.H., Soderblom, J.M., Hayes, A.G., Nicholson, P.D., 2011. Organic sedimentary deposits in Titan's dry lakebeds: probable evaporite. Icarus 216 (1), 136–140.

Bird, M.K. et al., 2005. The vertical profile of winds on Titan. Nature 438, 800–802.

Brown, G., Benney, R., 2005. Precision aerial delivery systems in a tactical environment, AIAA 2005–1645, 18th AIAA Aerodynamic Decelerator Systems Technology Conference and Seminar.

Brown, R.H., Lebreton, J.P., Waite, J.H. (Eds.), 2009. Titan from Cassini-Huygens. Springer Science & Business Media, New York.

Charnay, B., Lebonnois, S., 2012. Two boundary layers in Titan's lower troposphere inferred from a climate model. Nat. Geosci. 2012 (10.1038NGEO1374).

Clark, R.N., Curchin, J.M., Barnes, J.W., Jaumann, R., Soderblom, L., Cruikshank, D.P., Nicholson, P.D., 2010. Detection and mapping of hydrocarbon deposits on Titan. J. Geophys. Res.: Planets (1991–2012) 115 (E10).

Cornet, T., Bourgeois, O., Le Mouélic, S., Rodriguez, S., Lopez Gonzalez, T., Sotin, C., Nicholson, P.D., 2012a. Geomorphological significance of Ontario Lacus on Titan: integrated interpretation of Cassini VIMS, ISS and RADAR data and comparison with the Etosha Pan (Namibia). Icarus 218 (2), 788–806.

Cornet, T., Bourgeois, O., Le Mouélic, S., Rodriguez, S., Sotin, C., Barnes, J.W., Nicholson, P.D., 2012b. Edge detection applied to Cassini images reveals no measurable displacement of Ontario Lacus' margin between 2005 and 2010. J. Geophys. Res.: Planets (1991–2012) 117 (E7).

Coustenis, A., Taylor, F., 2008. Titan: Exploring an Earthlike World. World Scientific, Singapore (p. 412).

ESA, 2009. TSSM In-Situ Elements, Assessment Study Report, ESA-SRE(2008)4, European Space Agency, Noordwijk, The Netherlands, 12 February 2009 (http://sci.esa.int/science-e/www/object/doc.cfm?fobjectid=44184. downloaded 6th March 2015).

Flasar, F.M., Allison, M.D., Lunine, J.I., 1997. Titan zonal wind model. In: Huygens: Science, Payload, and Mission. In: Wilson, A. (Ed.), ESA SP-1177. European Space Agency, Noordwijk, pp. 287–298.

Flasar, F.M. et al., 2005. Titan's atmospheric temperatures, winds, and composition. Science 308, 975–978.

Flasar, F.M., Baines, K.H., Bird, M.K., Tokano, T., West, R.A., 2009. Atmospheric dynamics and circulation. In: Brown, R.H. et al. (Eds.), Titan from Cassini-Huygens. Springer, New York, pp. 323–352 (Chapter 13).

Folkner, W.M. et al., 2006. Winds on Titan from ground-based tracking of the Huygens probe. J. Geophys. Res. 111, E07S02.

Friedson, A.J., West, R.A., Wilson, E.H., Oyafuso, F., Orton, G.S., 2009. A global climate model of Titan's atmosphere and surface. Planet. Space Sci. 57, 1931–1949.

Hayes, A.G., Wolf, A.S., Aharonson, O., Zebker, H., Lorenz, R., Kirk, R.L., Paillou, P., Lunine, J., Wye, L., Callahanm, P., Wall, S., Elachi, C., 2010. Bathymetry and absorptivity of Titan's Ontario Lacus. J. Geophys. Res.: Planets 115 (E09009), 2010. http://dx.doi.org/10.1029/2009JE03557.

Hayes, A.G., Aharonson, O., Lunine, J.I., Kirk, R.L., Zebker, H.A., Wye, L.C., Lorenz, R.D., Turtle, E.P., Paillou, P., Mitri, G., Wall, S.D., Stofan, E.R., Mitchell, K.L., Elachi, C., 2011. Transient surface liquid in Titan's polar regions from Cassini. Icarus 211, 655–671 (the Cassini RADAR Team).

Haw, R.K., July 21–23, 2003 Approach Navigation for a Titan Aerocapture Orbiter. AIAA-2003-4802, 39th AIAA/ASME/SAE/ASEE Joint Propulsion Conference and Exhibit. Huntsville, Alabama.

JPL, 2010. Planetary Science Decadal Survey JPL Team X Titan Lake Probe Study. Final report. Jet Propulsion Laboratory, April 2010

(http://sites.nationalacademies.org/SSB/SSB_059331. downloaded 6th March 2015).

Knacke, T.W., 1991. Parachute recovery systems design manual No. NWC-TP-6575. US Naval Weapons center, China Lake, CA.

Leary, J., Jones, C., Lorenz, R., Strain, R.D., Waite, J.H., 2007. Titan Explorer NASA Flagship Mission Study, JHU Applied Physics Laboratory (public release version http://www.lpi.usra.edu/opag/Titan_Explorer_Public_Report.pdf downloaded January 2009).

Lebonnois, S., Burgalat, J., Rannou, P., Charnay, B., 2012. Titan global climate model: a new 3-dimensional version of the IPSL Titan GCM. Icarus 218, 707–722.

Lockwood, M.K., Leary, J.C., Lorenz, R., Waite, J.H., Reh, K., Prince, J., Powell, R., 2008. Titan Explorer, AIAA-2008-7071, AIAA/AAS Astrodynamics Specialist Conference, Honolulu, Hawaii, August 2008.

Lopes, R.M., Mitchell, K.L., Wall, S.D., Mitri, G., Kirk, R.L., Hayes, A.G., Aharonson, O., Stofan, E.R., Lunine, J.I., Lorenz, R.D., Wood, C., Radebaugh, J., Paillou, P., Janssen, M., Zebker, H. the Cassini RADAR Team, 2007. The Lakes and Seas of Titan. EOS 88, 569–570.

Lorenz, R.D., 2000. Post-cassini exploration of titan: science rationale and mission concepts. J. British Interplanet. Soc. 53, 218–234.

Lorenz, R.D., 2011. Apollo capsule capsize stability during splashdown: application of a cavity collapse model. J. British Interplanet. Soc. 64, 289–295.

Lorenz, R.D., 2015. Touchdown on venus: analytic wind models and a heuristic approach to estimating landing dispersions. Planet. Space Sci. 108, 66–72.

Lorenz, R.D., Mitton, J., 2010. Titan Unveiled. Princeton University Press, Revised Paperback edition.

Lorenz, R.D., Newman, C.E., Tokano, T., Mitchell, J., Charnay, B., Lebonnois, S., Achterberg, R., 2012a. Formulation of an engineering wind specification for titan late summer polar exploration. Planet. Space Sci. 70, 73–83.

Lorenz, R.D., Tokano, T., Newman, C.E., 2012b. Winds and tides of Ligeia Mare: application to the drift of the titan mare explorer (TiME) mission. Planet. Space Sci. 60, 72–85.

Lorenz, R.D., Kirk, R.L., Hayes, A.G., Anderson, Y.Z., Lunine, J.I., Tokano, T., Turtle, E.P., Malaska, M.J., Soderblom, J.M., Lucas, A., Karatekin, O., Wall, S.D., 2014. A radar map of Titan seas: tidal dissipation and ocean mixing through the throat of Kraken. Icarus 237, 9–15.

Mastroguiseppe, M., Poggiali, V., Hayes, A., Lorenz, R., Lunine, J., Picardi, G., Seu, R., Flamini, E., Mitri, G., Notarnicola, C., Paillou, P., Zebker, H., 2014. Bathymetry of a Titan sea. Geophys. Res. Lett. http://dx.doi.org/10.1002/2013GL058618.

Martin-Mur, T.J., Kruizingas, G.L., Burkhart, P.D., Wong, M.C., Abilleira, F., 2012, October. Mars science laboratory navigation results. In 23rd International Symposium on Space Flight Dynamics. Pasadena, California, October 29–November 2, 2012. Pasadena, CA. Jet Propulsion Laboratory, National Aeronautics and Space Administration, 2012.

Mitri, G., Coustenis, A., Fanchini, G., Hayes, A.G., Iess, L., Khurana, K., Lebreton, J.-P., Lopes, R.M., Lorenz, R.D., Meriggiola, R., Moriconi, M.L., Orosei, R., Sotin, C., Stofan, E., Tobie, G., Tokano, T., Tosi, F., 2014. The exploration of Titan with an orbiter and a lake probe. Planet. Space Sci. http://dx.doi.org/10.1016/j.pss.2014.07.009.

Newman, C.E., Lee, C., Lian, Y., Richardson, M.I., Toigo, A.D., 2011. Stratospheric superrotation in the TitanWRF model. Icarus 213, 636–654.

Pérez-Ayúcar, M., Lorenz, R.D., Floury, N., Prieto, R., Lebreton, J.-P., 2006. Surface properties of Titan from post-landing reflections of the huygens radio signal. J. Geophys. Res.: Planets 111 (E07001), 2006. http://dx.doi.org/10.1029/2005JE002613.

Reh, K.R., Elliott, J., 2010. Preparing for a future in situ mission to Titan. In: IEEE Aerospace Conference, Big Sky, MT., March 2010. 2007. doi:10.1109/AERO.2010.5446977.

Richardson, M.I., Toigo, A.D., Newman, C.E., 2007. PlanetWRF: a general purpose, local to global numerical model for planetary atmospheric and climate dynamics. J. Geophys. Res. 112, E09001.

Rogallo, F.M., 1967. NASA research on flexible wings. In: International Congress on Subsonic Aeronautics. NASA TMX-59738, New York, April 3–6.

Sicardy, B., 2006. The two Titan stellar occultations of 14 November 2003. J. Geophys. Res. 111, E11S91 (52 co-authors).

Sotin, C., Lawrence, K.J., Reinhardt, B., Barnes, J.W., Brown, R.H., Hayes, A.G., Le Mouélic, S., Rodriguez, S., Soderblom, J.M., Soderblom, L.A., Baines, K.H., Buratti, B.J., Clark, R.N., Jaumann, R., Nicholson, P.D., Stephan, K., 2012. Observations of Titan's Northern lakes at 5um: implications for the organic cycle and geology. Icarus 221, 768–786.

Space Studies Board. Vision and Voyages for Planetary Science in the Decade 2013–2022. National Academies Press, 2012 (http://solarsystem.nasa.gov/multimedia/download-detail.cfm?DL_ID=742, downloaded 6 March 2015).

Stein, J.M., Madsen, C.M., Strahan, A.L., 2005. An overview of the guided parafoil system derived from X-38 experience. AIAA-2005-1652 In: Proceedings of the 18th AIAA Aerodynamic Decelerator Systems Technology Conference and Seminar. Munich, Germany, May 2005, pp. 23–26.

Stofan, E.R., Elachi, C., Lunine, J.I., Lorenz, R.D., Stiles, B., Mitchell, K., Ostro, S., Soderblom, L., Wood, C., Zebker, H., Wall, S., Janssen, M., Kirk, R., Lopes, R., Paganelli, F., Radebaugh, J., Wye, L., Anderson, Y., Allison, M., Boehmer, R., Callahan, P., Encrenaz, P., Flamini, E., Francescetti, G., Gim, Y., Hamilton, G., Hensley, S., Johnson, W.T.K., Kelleher, K., Muhleman, D., Paillou, P., Picardi, G., Posa, F., Roth, L., Seu, R., Shaffer, S., Vetrella, S., West, R., 2007. The Lakes of Titan. Nature 441, 61–64.

Stofan, E., Lorenz, R., Lunine, J., Bierhaus, E., Clark, B., Mahaffy, P., Ravine, M., March 2013. TiME – The Titan Mare Explorer, IEEE Aerospace Conference, Big Sky, MT. paper #2434. doi: 10.1109/AERO.2013.6497165.

Tokano, T., Lorenz, R., Van Hoolst, T., 2014. Numerical simulation of tides and oceanic angular momentum of Titan's hydrocarbon seas. Icarus 242, 188–201.

Turtle, E.P. et al., 2009. Cassini imaging of Titan's high-latitude lakes, clouds, and south-polar surface changes. Geophys. Res. Lett. 36, L02204 (10.1029:2008GL036186).

Turtle, E., Perry, J.E., Hayes, A.G., Lorenz, R.D., Barnes, J.W., McEwen, A.S., West, R.A., Del Genio, A.D., Barbara, J.M., Lunine, J.I., Schaller, E.L., Ray, T.L., Lopes, R.M.C., Stofan, E.R., 2011a. Rapid and extensive surface changes near Titan's equator: evidence of April showers. Science 331, 1414–1417.

Turtle, E.P., Perry, J.E., Hayes, A.G., McEwen, A.S., 2011b. Shoreline retreat at Titan's Ontario Lacus and Arrakis Planitia from Cassini imaging science subsystem observations. Icarus 212 (2), 957–959.

Wall, S., Hayes, A., Bristow, C., Lorenz, R., Stofan, E., Lunine, J., Le Gall, A., Janssen, M., Lopes, R., Wye, L., Soderblom, L., Paillou, P., Aharonson, O., Zebker, H., Farr, T., Mitri, G., Kirk, R., Mitchell, K., Notarnicola, C., Casarano, D., Ventura, B., 2010. The active shoreline of Ontario Lacus, Titan: a morphological study of the lake and its surroundings. Geophys. Res. Lett. 37, L05202.

Witkowski, A., 2010. Evaluation of long term space effects on textiles from the Genesis Drogue parachute. In: IEEE Aerospace Conference. Big Sky, MT, March 2010. http://dx.doi.org/10.1109/AERO.2010.5447014.

## Further reading

Del Genio, A.D., Zhou, W., Eichler, T.P., 1993. Equatorial superrotation in a slowly rotating GCM: implications for Titan and Venus. Icarus 101, 1–17.